

Non-contacting ultrasonics for visualizing and exploiting multiple scattering

Alison E. Malcolm*, Center for Wave Phenomena and John A. Scales, Physical Acoustics Laboratory
Colorado School of Mines, Golden, CO.

Summary

Using lasers as both sources and detectors we are able to quickly collect large amounts of ultrasonic data on rock samples without the disturbances caused by contacting transducers. Since we excite primarily surface waves, recording the wavefield on the surface is analogous to measuring the wavefield within the scattering medium. Thus we can visualize wavefields as they propagate through rocks by watching the influence of scattering on the surface waves. To extract quantitative information about the rock sample, we fit the intensity data to a radiative transfer model. From this fit we extract the mean-free-path of the scattering, which gives us a measure of the scattering strength of the sample.

Introduction

An ultrasonic signal recorded in the laboratory consists of both ballistically traveling energy (energy traveling directly from the source to the receiver) and scattered energy that travels from the source to the receiver along more complicated paths. Typically information is obtained from the ballistic portion of the wavefield, and the later time signals are discarded as noise. This later, multiply scattered, signal often remains above the ambient noise level of the experiment, however, and thus contains information about the sample. (See Tourin et al. (2000) for a review of multiple-scattering theory.)

While contacting transducers work well for measuring properties from ballistic waves, collecting the amount of high quality data necessary to exploit the multiply scattered field with transducers is impractical. Also, the transducer itself acts as a scatterer, which interferes with the scattered field that we are interested in. Using lasers as both sources and receivers, we have recorded large data sets on aluminum, Elberton granite (fine-grained) and Llano granite (coarser-grained). Using these data we are able to visualize the wavefield, which helps us understand the origin of the sometimes complicated signals measured in the laboratory. By watching the wavefield propagate through samples with different scattering strengths we can see the influence of scattering on the wavefield.

Although watching the wavefield gives us a qualitative idea of the wave motion in the sample it does not yield a quantitative measure of the scattering strength. By using the radiative transfer equation (Paasschens, 1997) as a model of energy transport in a scattering medium, we can extract the mean-free-path from the data. The mean-free-path is a parameter that is used in many areas of physics as a measure of scattering strength.

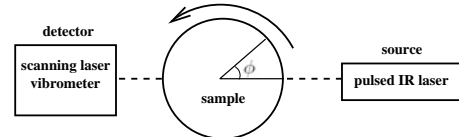


Fig. 1: Experimental configuration for the rotational scan experiment.

Experimental Setup

In our laboratory, we study ultrasonic wave propagation in heterogeneous media such as rocks and engineered composites. A pulsed Nd:YAG laser (1064-nm wavelength, 5-ns pulses, .3 J/pulse) is used to excite ultrasonic waves via thermoelastic expansion or ablation. That is, the source laser heats up a small (a few mm²) region of the sample causing thermoelastic expansion, which sends waves through the sample. These waves are detected using a scanning laser interferometer that measures the absolute particle velocity on the surface of the sample via the Doppler shift. (See Scruby and Drain (1990) for the general principles of laser vibrometry.) The output of the interferometer is then digitized at 14-bit precision using a digital oscilloscope card attached to a PC. The lasers and the sample are positioned on an optical bench with vibration isolation. The dominant frequency of the measured waves is 1 MHz, a limit imposed by the detector electronics. (At GHz frequencies, femtosecond lasers have recently been used to visualize ultrasound propagation in crystalline material (Sugawara et al., 2002) by scanning the surface.)

We show results here from three different experiments (see Scales and Malcolm (2003) for more details). The first is a rotational scan; a cylindrical sample is positioned between the source and receiver lasers and measurements are made as a function of ϕ , the orientation of the sample relative to the line on which the source and receiver lie (see Figure 1). We use this experimental configuration to illustrate the length of time over which we see coherent signal and to illustrate the influence of scattering strength on the early time field. The second experiment, which we refer to as a surface scan, consists of data collected on the top (circular) surface of cylindrical samples. The data are collected on a dense grid, allowing us to visualize them at high resolution. Using these data we are able to watch the energy distribute through the sample as a result of the scattering. The final experiment is a surface scan made of a rectangular region on a large block of granite, with the source laser focused on a line. This experiment

Laser Measurement of Multiple Scattering

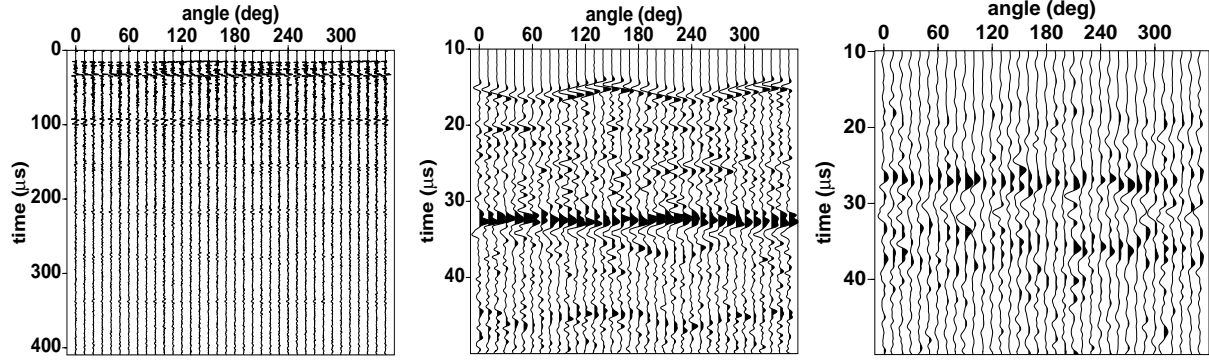


Fig. 2: Data from a rotational scan. On the left is data collected on the Elberton granite with no gain applied; the flat events are whispering gallery and Rayleigh waves, six of which are visible in this figure. The middle figure is a zoom of the early signal. The first-arriving energy is the direct P-wave which shows the approximately 10% anisotropy of the sample. The flat Rayleigh wave at about 33 μ s is split because of heterogeneity along the path; it is the sum of two interfering waves, one traveling in each direction around the sample. This splitting is accentuated in the data on the right collected on the Llano granite, which has coarser grains and thus stronger scattering. The first-arriving P-wave is so strongly attenuated by the scattering in this sample that is not visible on this plot.

was performed to eliminate edge effects seen in the surface scans of the cylindrical samples, allowing us to draw more quantitative conclusions from the data.

We show data from experiments on two different granite samples. The two samples have similar attenuation properties (measured with resonance ultrasound spectroscopy (Zadler et al., 2002)), anisotropy, and average velocities. The Elberton granite has small grains and thus weak scattering, while the Llano granite is a coarser grained rock and so has stronger scattering. The cylindrical Elberton granite sample is 55 mm in diameter and the Llano sample is 50 mm in diameter.

Data and Analysis

Figure 2 shows the data for the rotational scan. In the Elberton granite, the scattering is weak enough that surface waves can travel around the sample many times (we have recorded up to 10 circumnavigations). In the zoom of the Elberton data, we can clearly see the first-arriving P-waves as well as a strong surface wave. By contrast, the Llano data shown on the right side of the figure show very weak first arrivals and we see more splitting between the two counter-rotating surface waves caused by the stronger scattering.

By looking at the data from the surface scan experiment, shown in Figure 3 we gain a clearer picture of the scattering. We performed this experiment on three samples, adding aluminum to help us understand what to expect in a homogeneous medium. In aluminum, it is possible to watch coherent arrivals propagate for a long time; we can follow the surface waves on the circular edges throughout the recording time. In the Elberton granite, we see sev-

eral reflections of the surface wave from the edges of the boundary as well as coherent surface waves along the edge of the sample for most of the recording time. This indicates that the scattering in the Elberton granite is quite small as we suspected from the rotational scan data. In the Llano granite however, the data quickly decay to incoherent speckle; it is difficult to follow the surface wave after only one reflection from the edge. The attenuation properties of the two granites are similar, so the differences in the properties of the waveforms are due almost entirely to scattering.

Thus far, we have shown that the wavefield changes in the presence of grain scattering. The differences between the wavefields in the three samples are obvious to the eye. (These differences are even clearer in movie form, available at <http://acoustics.mines.edu>.)

Although we can see the effects of grain scattering on the wavefield, the small size of the samples discussed thus far is a problem because scattering from the grains is intermixed with scattering from the edges of the samples, making the grain scattering difficult to separate from edge reflections.

If it can be separated from the edge reflections, however, the scattered field can yield information about the structure of the sample. To do this, we collected data on a large ($8 \times 4 \times 160$ cm 3) block of the Llano granite. Because of the relatively large size of the sample, we do not expect its edges to influence the data. In this experiment, we focus the source laser on a line so that when we collect data in a rectangular region in front of the source, each line perpendicular to the source is essentially the same experiment, allowing us to stack the data. Using these data, we fit the two-dimensional radiative transfer

Laser Measurement of Multiple Scattering

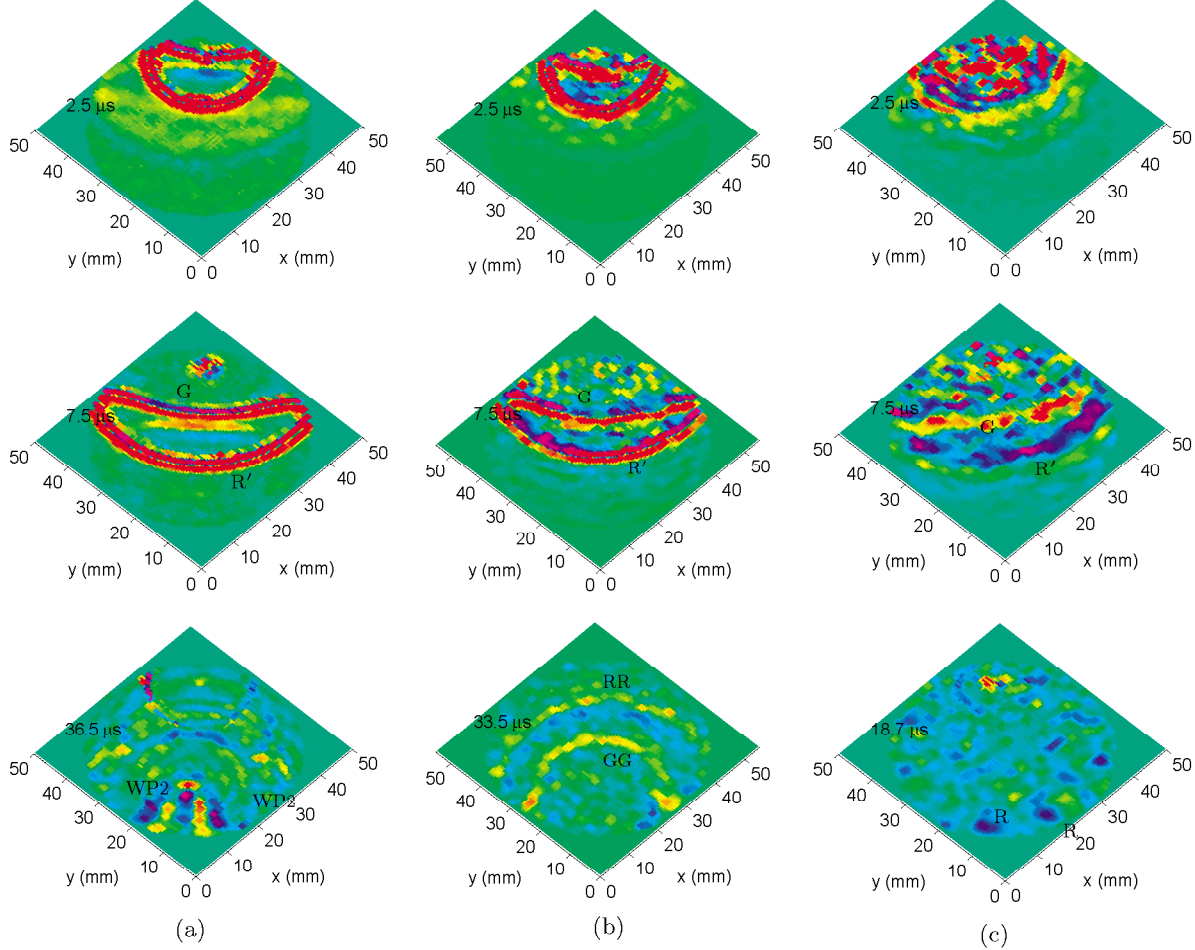


Fig. 3: Snapshots of the wavefield measured on one end of the cylinder. (Color figures are available in Scales and Malcolm (2003)) The source laser is focused on a point 7 mm from the edge of the cylinder, on the end on which data are collected. Although the surface wavefields (Rayleigh waves) dominate the data, both compressional and shear body waves are visible as well as Rayleigh and whispering gallery waves propagating around the edge of the cylinder. In the snapshots, G refers to the so-called ghost wave, which is a reflection of the source from the side of the sample. R' is a Rayleigh wave on the end of the sample, R is a Rayleigh wave propagating around the circular edge, WP are whispering gallery P-modes (WP2 has traveled one and a half times around the outside edge of the sample). (a) Data collected on an aluminum sample. (b) Data collected on the fine-grained Elberton granite. (c) Data collected on the coarser grained llano sample. Notice the difference in the characteristics of the wavefield among the three samples.

equation (Paasschens, 1997)

$$I(r, t) = e^{-ct(1/\ell_a + 1/\ell_s)} \left(\frac{\delta(ct - r)}{2\pi r} + \frac{1}{2\pi\ell_s\sqrt{1 - \frac{r^2}{c^2 t^2}}} e^{\frac{ct}{\ell_s}\sqrt{1 - \frac{r^2}{c^2 t^2}}} H(ct - r) \right), \quad (1)$$

where c is the energy velocity, r is the distance from the source, t is the time, ℓ_s is the scattering mean-free-path, ℓ_a is the attenuation mean-free-path (related to the quality factor Q), H is the Heaviside function and $I(r, t)$ is

the total intensity. The scattering mean-free-path is the time at which the intensity has decayed, as a result of scattering, to a factor $1/e$ of its original amplitude. For discrete scatters (which grains in a rock are not) this distance corresponds to the distance between the scatters. The total intensity is the sum of the squares of all the traces in the ensemble. In this experiment, the ensemble is the set of lines of data collected perpendicular to the line source. This model assumes no mode conversion or wave localization and that the scattering is isotropic.

The Dirac delta function term in the radiative transfer equation models the ballistic wave propagation, which is strongly influenced by the distance from the source. The

Laser Measurement of Multiple Scattering

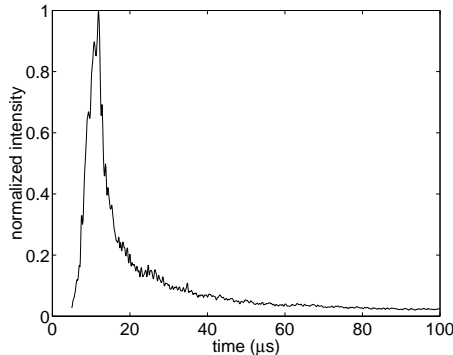


Fig. 4: Once the coherent pulse has passed the detector (i.e., after about $15 \mu\text{s}$) the total intensity is essentially independent of distance within the scan region. The intensity, averaged over source-to-detector distance, is shown here. The broad peak in this figure is the result of averaging the ballistic energy over different distances.

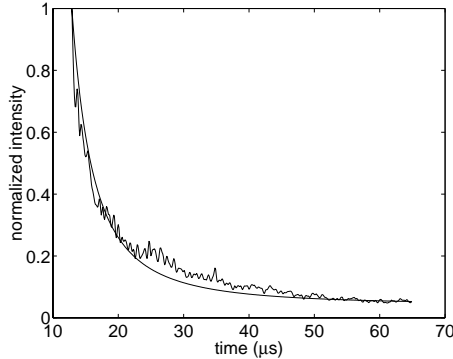


Fig. 5: A radiative transfer fit to the late-time intensity for the scattering mean-free-path of 8 mm. Analysis of the optimization problem for ℓ_s gives an uncertainty of about ± 2 mm.

second term in the equation models the scattered energy. At late time, $t \gg r$ and so this second term is essentially independent of r . We take advantage of this fact to reduce the variation in our data by stacking over r as well as over the different receiver lines (i.e., we increase the number of traces in our ensemble by adding all traces together not just those with the same perpendicular distance from the source). This total intensity is shown in Figure 4. In this figure, the averaging over r has lead to a broad peak centered at about $15 \mu\text{s}$, which is the result of averaging the ballistic energy over distance. In Figure 5, these data are fit to the radiative transfer equation to extract the scattering mean-free-path of this sample. From this fit we obtain a value of 8 ± 2 mm for the scattering mean-free-path. Because of the strong scattering, our data do not constrain the absorption, however it is possible to use the radiative transfer model to separate intrinsic and scattering absorption if neither dominates.

Conclusions

Exploiting multiple scattering to determine properties of rocks requires large amounts of high-quality data. Collecting such data with ultrasonic transducers is impractical because of the large number of receiver positions required and the interference of transducers with the measured field. Using lasers as both sources and detectors alleviates this problem by allowing the focusing of sources on lines, or regions much smaller than the smallest transducer and by allowing data to be collected at many more receiver locations than would be possible with contacting transducers. We have shown how these measurement methods allow us to see the influence of scattering on the wavefield, giving us greater insight into scattering dynamics. Also, we are able to extract the mean-free-path of the strongly scattering Llano granite, giving a quantitative measure of its scattering strength. Thus, we have been able to extract information about the small-scale structure of the rock from the late-time wavefield that is commonly discarded as noise.

References

- Paasschens, J. C., 1997, Solution of the time-dependent boltzmann equation: Phys. Rev. E, **56**, 1135.
- Scales, J. A., and Malcolm, A. E., 2003, Laser characterization of ultrasonic wave propagation in random media: in press, Phys. Rev. E.
- Scruby, C., and Drain, L., 1990, Laser ultrasonics: techniques and applications: Adam Hilger.
- Sugawara, Y., Wright, O. B., Matsuda, O., Takigahira, M., Y. Tanaka, S. T., and Gusev, V. E., 2002, Watching ripples on crystals: Phys. Rev. Lett., **88**, 185504.
- Tourin, A., Fink, M., and Derode, A., 2000, Multiple scattering of sound: Waves Random Media, **10**, R31.
- Zadler, B., Le Rousseau, J. H., Scales, J. A., and Smith, M. L., 2002, Resonant ultrasound spectroscopy: theory and application: preprint.

Acknowledgements

We acknowledge many useful discussion with Bart Van Tiggelen, of Université Joseph Fourier in Grenoble and with our CSM colleagues Roel Snieder, Kasper van Wijk, Alex Grêt, Matt Haney, Huub Douma, and Carlos Pacheco. This work was partially supported by the National Science Foundation (EAR-0111804), US Army Research Office (DAAG55-98-1-0070), TotalFinaElf, and the sponsors of the Consortium Project on Seismic Inverse Methods for Complex Structures at the Center for Wave Phenomena.